# Dynamic scaling of order parameter fluctuations in model B

Chandrodoy Chattopadhyay,[1] Josh Ott,[1] Thomas Schäfer,[1] and Vladimir Skokov[1,2]
[1]*Department of Physics, North Carolina State University, Raleigh, North Carolina 27695, USA*
[2]*RIKEN BNL Research Center, Brookhaven National Laboratory, Upton, New York 11973, USA*

(Received 28 April 2023; accepted 11 September 2023; published 5 October 2023)

We describe numerical simulations of the stochastic diffusion equation with a conserved charge. We focus on the dynamics in the vicinity of a critical point in the Ising universality class. The model we consider is expected to describe the critical dynamics near a possible QCD critical point if the coupling of the order parameter to the momentum density of the fluid can be neglected. The simulations are performed on a spatial lattice, and the time evolution is performed using a Metropolis algorithm. We determine the dynamical critical exponent $z \simeq 3.972(2)$, which agrees with predictions of the epsilon expansion. We also study nonequilibrium sweeps of the reduced temperature and observe approximate Kibble-Zurek scaling.

DOI: 10.1103/PhysRevD.108.074004

## I. INTRODUCTION

Understanding the dynamical evolution of fluctuations in the vicinity of a critical point in the phase diagram is crucial for interpreting the data from the Beam Energy Scan (BES) program at the Relativistic Heavy-Ion Collider (RHIC) at Brookhaven National Laboratory [1–4]. Given the success of the fluid dynamic description of heavy-ion collisions at RHIC, it is natural to assume that the dynamics of fluctuations can also be understood in a fluid dynamic framework. The relevant fluid dynamic theories are relativistic generalizations of the hydrodynamic models classified by Hohenberg and Halperin [5]. This includes purely relaxational dynamics (model A) [6,7], the dynamics of a conserved order parameter (model B) [8–10], a conserved order parameter coupled to the momentum density of the fluid (model H) [11], and the dynamics of a chiral order parameter (model G) [12–14]. Ultimately, the dynamics near a possible critical endpoint in the QCD phase diagram is expected to be governed by model H [11], but in the present work we neglect the coupling to the momentum density of the fluid and focus on model B. This work builds on our earlier study of model A [7].

There are two main approaches to fluid dynamic theories with fluctuations. The first is based on performing the noise average analytically, and deriving a set of deterministic evolution equations for $n$-point functions or $n$th order cumulants of hydrodynamic variables [15–22]. This approach is sometimes described as the hydrokinetic or Hydro+ method. The second option is to simulate the equations of stochastic fluid dynamics [6,7,9,10,23,24]. The advantage of the deterministic method is that the issue of regularization and renormalization of short-distance noise can be handled analytically. The main advantage of stochastic simulations is that there is no need for additional approximations. Commonly used approximations include the truncation of hierarchies of correlation functions, as well as models for equilibrium two-point functions and relaxation rates.

In the present work we follow the second approach and study the stochastic dynamics of a conserved order parameter in the vicinity of a phase transition in the universality class of the Ising model. We employ a simple algorithm based on the Metropolis method [7,14]. Our goal is to demonstrate the efficacy of this algorithm in the case of a fluid dynamic theory with a conserved charge. We focus, in particular, on the dynamical critical exponent, and on the observation of Kibble-Zurek scaling for nonequilibrium sweeps of the parameters of the theory [25–27]. The long-term objective is to further generalize the methods presented in this work to model H, and to couple the dynamics to a nontrivial background flow.

## II. MODELS A AND B

Consider a scalar field $\phi(t,\vec{x})$ which evolves according to a stochastic relaxation equation,

$$\partial_t \phi(t,\vec{x}) = -\hat{\Gamma}_{A,B} \frac{\delta \mathcal{H}}{\delta \phi(t,\vec{x})} + \zeta(t,\vec{x}). \tag{1}$$

For purely relaxational dynamics (model A) $\hat{\Gamma}_A = \Gamma > 0$ is a constant. In the case of a conserved order parameter (model B) the relaxation rate is proportional to $\nabla^2$, i.e., $\hat{\Gamma}_B = -\Gamma\nabla^2$. The Hamiltonian $\mathcal{H}$ is given by

$$\mathcal{H} = \int d^d x \left[ \frac{1}{2}(\nabla\phi)^2 + \frac{1}{2} m^2 \phi^2(t,\vec{x}) + \frac{1}{4}\lambda\phi^4(t,\vec{x}) - h(t,\vec{x})\phi(t,\vec{x}) \right], \tag{2}$$

 

where $m$ is the bare inverse correlation length, $\lambda$ is the self-coupling, and $h$ is an external field. The noise term $\zeta(t,\vec{x})$ is a random field constrained by fluctuation-dissipation relations. This determines the correlation function of the noise

$$\langle\zeta(t,\vec{x})\zeta(t',\vec{x}')\rangle = 2T\hat{\Gamma}_{A,B}\delta(\vec{x}-\vec{x}')\delta(t-t'). \quad (3)$$

In order to perform numerical simulations we discretize the Hamiltonian on a lattice with lattice spacing $a$. We use periodic boundary conditions on a cubic lattice with sides of length $L = Na$, and we adopt units so that $a = 1$. The discretized Hamiltonian is

$$\mathcal{H} = \sum_{\vec{x}}\left[\frac{1}{2}\sum_{\mu=1}^{d}(\phi(\vec{x}+\hat{\mu})-\phi(\vec{x}))^2 + \frac{1}{2}m^2\phi^2(\vec{x}) + \frac{1}{4}\lambda\phi^4(\vec{x}) - h\phi(\vec{x})\right], \quad (4)$$

where we have suppressed the time argument of the field $\phi(\vec{x})$, and the sum over $\vec{x}$ is a sum over integer vectors $\vec{n}$ so that $\vec{x} = a\vec{n}$. We also define a unit vector $\hat{\mu}$ in the direction $\mu \in \{1,\ldots,d\}$, where $d$ is the number of spatial dimensions. In the present work we will only consider $d = 3$.

In order to study time evolution we have to determine the change in the Hamiltonian for an update of the field. In model A the update is purely local. Changing the field $\phi_{\text{old}} \to \phi_{\text{new}}$ at a fixed position $\vec{x}$ leads to

$$\begin{aligned}\Delta\mathcal{H}(x) = {} & d(\phi^2_{\text{new}}(\vec{x}) - \phi^2_{\text{old}}(\vec{x})) \\ & - (\phi_{\text{new}}(\vec{x}) - \phi_{\text{old}}(\vec{x}))\sum_{\mu=1}^{d}(\phi(\vec{x}+\hat{\mu}) + \phi(\vec{x}-\hat{\mu})) \\ & + \frac{1}{2}m^2(\phi^2_{\text{new}}(\vec{x}) - \phi^2_{\text{old}}(\vec{x})) + \frac{1}{4}\lambda(\phi^4_{\text{new}}(\vec{x}) \\ & - \phi^4_{\text{old}}(\vec{x})) - h(\phi_{\text{new}}(\vec{x}) - \phi_{\text{old}}(\vec{x})). \end{aligned} \quad (5)$$

In model B the order parameter is conserved, and an update involves two adjacent sites at the position $x$ and $x+\hat{\nu}$. The change in Hamiltonian is

$$\begin{aligned}&\Delta\mathcal{H}(x, x+\hat{\nu}) \\ &\quad = \Delta\mathcal{H}(x) + \Delta\mathcal{H}(x+\hat{\nu}) \\ &\qquad - (\phi_{\text{new}}(\vec{x}) - \phi_{\text{old}}(\vec{x}))(\phi_{\text{new}}(\vec{x}+\hat{\nu}) - \phi_{\text{old}}(\vec{x}+\hat{\nu})),\end{aligned} \quad (6)$$

where, for a conserved field, we have $q \equiv \phi_{\text{new}}(\vec{x}) - \phi_{\text{old}}(\vec{x}) = -[\phi_{\text{new}}(\vec{x}+\hat{\nu}) - \phi_{\text{old}}(\vec{x}+\hat{\nu})]$, so that the last term in Eq. (6) is equal to $+q^2$.

### A. Model A update

Following our earlier work [7] as well as the recent publication by Florio *et al.* [14] we study the stochastic evolution using the Metropolis method. The basic observation is that one can use a single Metropolis step to implement both the diffusive and the stochastic terms in the equation of motion. There is some rigorous work on this method in the mathematics literature [28], but it has not been used widely in either mathematics or physics. For some exceptions, see [29,30] as well as [31,32]. The time evolution is discretized using a fixed time step size $\Delta t$. We perform a checkerboard sweep through the spatial lattice. The checkerboard consists of even lattice sites (the A lattice) and odd lattice sites (the B lattice). For every site $\vec{x} \in$ A we perform a trial update

$$\phi_{\text{new}}(\vec{x}) = \phi_{\text{old}}(\vec{x}) + \sqrt{2\Gamma\Delta t}\,\xi. \quad (7)$$

Here $\xi$ is a random number drawn from a Gaussian distribution with zero mean and variance one. The trial update is accepted with probability $P = \min(1, e^{-\Delta\mathcal{H}/T})$. In this case, we update the field as

$$\phi(t+\Delta t,\vec{x}) = \phi_{\text{new}}(\vec{x}). \quad (8)$$

If the trial update is rejected then the field is not changed. This update implies that

$$\langle\phi(t+\Delta t,\vec{x}) - \phi(t,\vec{x})\rangle = -(\Delta t)\Gamma\frac{\delta\mathcal{H}}{\delta\phi} + O((\Delta t)^2), \quad (9)$$

$$\langle[\phi(t+\Delta t,\vec{x}) - \phi(t,\vec{x})]^2\rangle = 2(\Delta t)\Gamma T + O((\Delta t)^2). \quad (10)$$

The first moment ensures that the deterministic part of Eq. (1) is satisfied, and the second moment reproduces the variance of the stochastic force in the equation of motion.

The same procedure is repeated for all points in the B lattice. For the nearest neighbor interaction in Eq. (4) the updates of all $\vec{x} \in$ A are independent of each other, and can be performed in parallel. The same is true for updates in the B lattice. An important property of the procedure is that the probability of obtaining a new configuration $(\phi^A_{\text{new}}, \phi^B_{\text{new}})$, where $\phi^{A,B}$ are the fields on the A, B sublattices, only depends on the difference in the Hamiltonian of the initial and final states

$$\begin{aligned}&P((\phi^A,\phi^B) \to (\phi^A_{\text{new}},\phi^B_{\text{new}})) \\ &\quad \sim \exp\left(-[\mathcal{H}(\phi^A_{\text{new}},\phi^B_{\text{new}}) - \mathcal{H}(\phi^A,\phi^B)]/T\right),\end{aligned} \quad (11)$$

and not on the order in which the updates are performed, or on the intermediate values of the fields. We also note that the detailed balance condition is satisfied irrespective of the size of the time step. This means that the Metropolis algorithm defined by Eqs. (7) and (8) samples the equilibrium distribution $P[\phi] \sim \exp(-\mathcal{H}[\phi]/T)$ even if $\Delta t$ is not small. In contrast, if $\Delta t$ is not small then the model A dynamics in Eq. (1) is only realized approximately. However, because the model A/B equation represents the

general low energy approximation to relaxational dynamics in the absence/presence of a conservation law, the leading effect of a nonzero $\Delta t$ is to modify the value of the relaxation rate.

### B. Model B update

In the case of model B we wish to ensure that the update of the field respects the conservation law exactly. For this purpose we write the equation of motion in the form

$$\partial_t \phi + \overrightarrow{\nabla} \cdot \vec{j} = 0, \qquad \vec{j} = -\Gamma \overrightarrow{\nabla} \frac{\delta \mathcal{H}}{\delta \phi} + \vec{\xi}, \tag{12}$$

with

$$\langle \xi_i(\vec{x}, t) \xi_j(\vec{x}', t') \rangle = \delta_{ij} \Gamma T \delta(\vec{x} - \overrightarrow{x'}) \delta(t - t'). \tag{13}$$

Equation (12) can be integrated over a cell centered on $\vec{x} = a\vec{n}$. The integral of $\phi$ over a cell is $\phi_c(\vec{x}) = a^d \phi(\vec{x})$ and in units $a = 1$ there is no need to distinguish between $\phi_c$ and $\phi$. The evolution equation for $\phi = \phi_c$ is

$$\partial_t \phi = -\sum_{\mu=1}^{d} (q_\mu^+ - q_\mu^-), \tag{14}$$

where $q_i^\pm$ are the fluxes through the forward and backward faces of the cube centered on $\vec{x} = a\vec{n}$ in the Cartesian $i$-direction. We can use the Metropolis algorithm discussed in the previous section to update the fluxes. A trial update for the cells $(\vec{x}, \vec{x} + \hat{\mu})$ is

$$\begin{aligned} \phi_{\text{new}}(\vec{x}) &= \phi_{\text{old}}(\vec{x}) + q_\mu, \\ \phi_{\text{new}}(\vec{x} + \hat{\mu}) &= \phi_{\text{old}}(\vec{x} + \hat{\mu}) - q_\mu, \end{aligned} \qquad q_\mu = \sqrt{2\Gamma \Delta t}\xi. \tag{15}$$

The update is accepted with probability $\min(1, e^{-\Delta \mathcal{H}})$.

In the case of the conserving update in Eq. (15) it is more complicated to construct a checkerboard algorithm. The update involves two cells, and for a nearest-neighbor Hamiltonian these two cells have $4d - 2$ neighbors. We use a fourfold checkerboard which is repeated in all $d$ directions to update all interfaces while avoiding interference between neighboring cells. This ensures that the detailed balance condition Eq. (11) is satisfied.

Two stages of the algorithm are shown in the left and right panel of Fig. 1. The figure shows a two-dimensional slice in the $(ij)$ plane of a three dimensional lattice labeled by $(xyz) = (ijk)$. In the two stages shown every pair of green cells is updated by applying a stochastic flux at the interface in $i$ direction. The figure is replicated in the $k$ direction by alternating green and blue cells. All these updates can be performed in parallel. Stages three and four correspond to repeating the procedure with green and blue cells interchanged. After these four stages are complete all interfaces in the $x = i$ direction have been updated. The process is then repeated for all right-handed permutations of $x$, $y$, and $z$

$$(i, j, k) \to (x, y, z), (y, z, x), (z, x, y). \tag{16}$$

This completes a full update of the lattice. As in the case of model A the update satisfies detailed balance exactly, even for finite $\Delta t$. However, the diffusion equation is only realized up to correction of higher order in $\Delta t$.

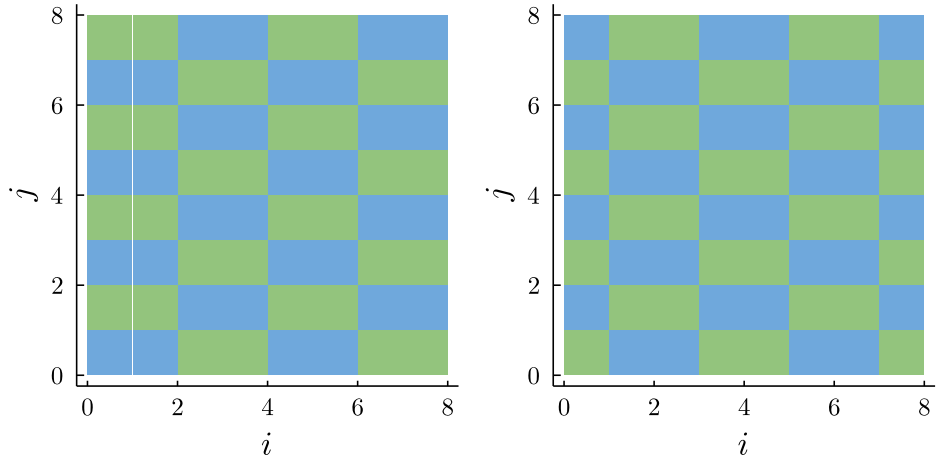


FIG. 1. Checkerboard algorithm for a conserving (model B) update. For illustration we show two stages (left and right panel) of the algorithm acting on one plane of a three-dimensional lattice of size $L = 8$ labeled by indices $(ijk)$. In the first stage (left panel) pairs of green cells are updated by applying a stochastic flux at their interface. Blue cells are unmodified. In the $k$-direction (not shown) alternate layers have green and blue cells interchanged. In the second stage (right panel) the update is applied to a shifted set of cells. Stages three and four correspond to exchanging green and blue cells relative to stage one and two. Finally, the same pattern is applied in the $(j, k)$ and $(k, i)$ plane.

## III. NUMERICAL SIMULATIONS

Numerical simulations of model A dynamics were described in our previous work [7]. In that work we used Binder cumulants to determine the critical value of $m^2$ at which the second order phase transition takes place. For $\lambda = 4$ we obtained $m_c^2 = -2.28587(7)$. Since static properties of model B are identical to those of model A, this result directly carries over to the present work. As we will discuss in more detail below, there is a caveat related to the fact that static correlation functions in a finite volume are affected by global conservation laws. In particular, in our model B simulations the total charge is always zero, whereas the total charge fluctuates in simulations of model A.

In this section we first study the correlation function directly at the critical point $m_c^2$, where the correlation length in the thermodynamic limit diverges. In a finite volume the correlation length is limited by the system size $L$, and we can use this dependence to analyze dynamical scaling. We then investigate the correlator at $m^2 \neq m_c^2$ and extract the correlation length and relaxation time away from the critical point. In Sec. IV we study nonequilibrium sweeps, and in this case the correlation length is limited by critical slowing down. Note that we have set $a = 1$, and all lengths are measured in units of the lattice spacing. We have also used $\Gamma = 1$, and the unit of time is given by $a^4/\Gamma$. Finally, we have set $T = 1$, and the magnetization $\langle\phi\rangle$ is given in units $T/a^{1/2}$.

The dynamic correlation function of the density is defined by

$$G(t,\vec{k}) = \int d^3x\, e^{i\vec{k}\cdot\vec{x}} \langle\phi(0,0)\phi(\vec{x},t)\rangle. \tag{17}$$

In Fig. 2 we show this function for the lowest nontrivial lattice momentum at the critical point for four different lattice volumes. Critical scaling predicts that correlation functions obtained in different volumes collapse to a universal function if the time argument is scaled by $L^z$, where $z$ is the dynamic critical exponent of model B. In Fig. 2 we show that data collapse occurs for $z = 3.972$. A more detailed analysis of the dynamic critical exponent is shown in Fig. 3. For different values of $L$ we show the relaxation time extracted from a fit $G(t,\vec{k}) \sim e^{-t/\tau}$ where $\vec{k} = (2\pi/L, 0, 0)$. We observe that the dependence of $\log(\tau)$ on $\log(L)$ is linear, and from the slope of this relation we determine the value $z = 3.972$. We can get an estimate of finite $L$ corrections by excluding the smallest $L$-value, $L = 8$, from the fit. In this case we get $z = 3.970$, and we conclude that $z = 3.972(2)$. Other sources of error are more difficult to quantify. As mentioned above there is a (small) uncertainty in the determination of $m_c^2$, and we have not attempted to quantify the impact of this error on the measurement of $z$. We can compare our result $z = 3.972(2)$ to the theoretical prediction of $z = 4 - \eta$ [5], where $\eta$ is the static correlation function exponent defined by $G(0,|\vec{k}|) \sim 1/|\vec{k}|^{2-\eta}$. In the $\epsilon$ expansion $\eta = 3\epsilon^2/162 \simeq 0.019$ [33], and in the conformal bootstrap $\eta \simeq 0.0363$ [34,35]. Based on the latter result we expect $z \simeq 3.96$, in good agreement with our result.

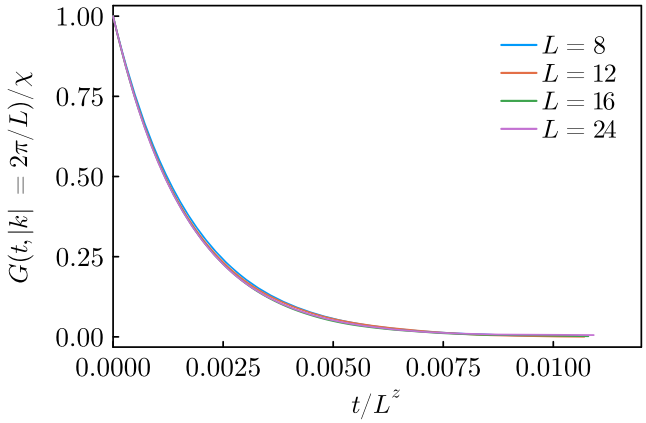


FIG. 2. Dynamic density-density correlation function $G(t,\vec{k})$ for the lowest lattice momentum $\vec{k} = (2\pi/L, 0, 0)$. We show the results obtained in three different volumes with linear size $L = 8$, 12, 16, 24. Pale bands indicate the statistical error of the data. The time variable is scaled by $L^z$ with $z = 3.972$. The correlation function is normalized to $\chi = G(0, 2\pi/L)$.

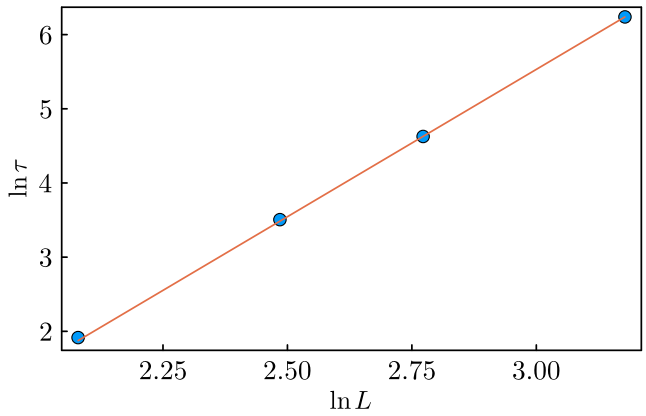


FIG. 3. Relation between the decay time $\tau$ extracted from the correlation function $G(t,|\vec{k}| = 2\pi/L)$ and the linear box size $L$. The line shows the best fit with $z = 3.972$.

We note that the large value of $z$ implies that configurations in model B are very difficult to thermalize. The effort to update a single configuration scales like the volume $V \sim L^3$, and the number of updates required to thermalize the system scales as $L^z \sim L^4$. This implies that at the critical point the effort scales roughly as $L^7$. Away from the critical point stochastic simulations are significantly faster.

We have also studied correlation functions away from the critical point $m^2 = m_c^2$. In Fig. 4 we show the correlation length extracted from a fit to the equal-time correlation function $G(0,\vec{x})$. In particular, we write

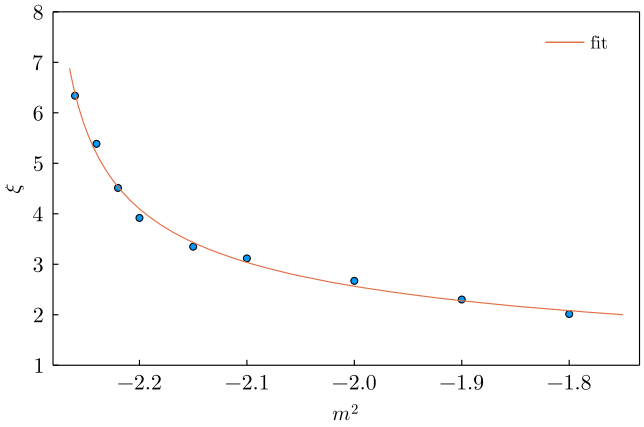


FIG. 4. Model B correlation length $\xi$ as a function of the bare mass parameter $m^2$. We also show a fit $\xi \sim 1/(m^2 - m_c^2)^\nu$ with $\nu = 0.542$ and $m_c^2 = -2.267$.

$G(0, \vec{x}) \sim x^{-1} \exp(-x/\xi)$ with $x = |\vec{x}|$ and fit $\xi$ to the measured correlation function in the regime $x < L/2$. In practice, the fit window has to be smaller, because conservation of total charge implies that the model B correlation function at $x \sim L/2$ is negative. Indeed, we find that because of finite size corrections the model B correlation length in any finite system is smaller than the one in model A, even though the two theories are governed by the same static universality class. We have fitted the correlation lengths shown in Fig. 4 to a power law $\xi \sim 1/(m^2 - m_c^2)^\nu$. We find $m_c^2 = -2.267$ and $\nu = 0.542$. The value of $m_c^2$ is consistent with (but much less precise than) the value $m_c^2 = -2.28587(7)$ extracted from the Binder cumulants. Similarly, because of finite size effects, the value of $\nu$ is consistent with the expectation $\nu = 0.6299(5)$ [34], but not very precise.

In Fig. 5 we show the dependence of the relaxation time on the bare mass parameter $m^2$. The relaxation time is extracted for the lowest Fourier mode $k = 2\pi/L$ by using a simple exponential fit $G(t, k = 2\pi/L) \sim \exp(-t/\tau)$. Figure 5 clearly demonstrates that the variation of the relaxation time with $m^2$ is much more dramatic than that of the correlation length. A simple fit of the form $\tau \sim \xi^z$ gives $z \simeq 3.73$. This fit is consistent with, but not nearly as accurate, as the determination of $z$ from finite-size scaling at the critical point $m^2 = m_c^2$ shown in Fig. 3.

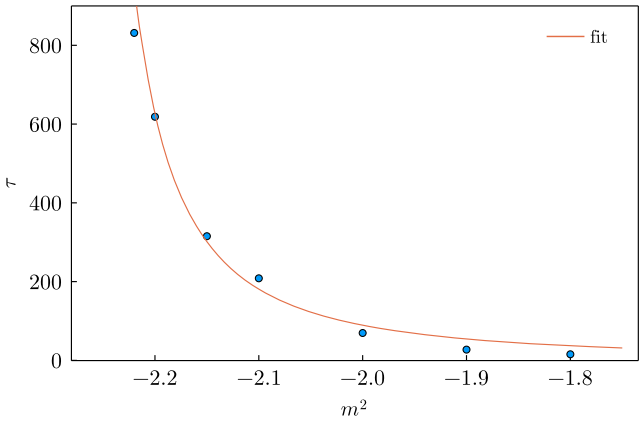


FIG. 5. Model B relaxation time $\tau$ as a function of the bare mass parameter. Here, $\tau$ is measured for the lowest nontrivial Fourier mode $k = 2\pi/L$. We also show the best fit $\tau \sim \xi^z$ with $z \simeq 3.73$.

## IV. KIBBLE-ZUREK SCALING

In practical applications of stochastic diffusion we are often interested in far-from-equilibrium dynamics. In our previous work on the dynamics of model A we studied quench dynamics [7]. We equilibrated the system in the high-temperature phase, and performed an instantaneous sweep to the critical point. We then studied the evolution of moments of the order parameter towards their equilibrium values at the critical point.

In this section we study a different situation. We again equilibrate the system in the high temperature phase, but then sweep towards the critical regime at a finite rate. Because of critical slowing down, correlation functions drop out of equilibrium as the critical point is approached. This behavior can be characterized in terms of a time scale, the Kibble-Zurek time $\tau_{KZ}$ [16,19,25–27,36]. This is the time at which fluctuations on a length scale defined by the instantaneous correlation length $\xi$ are no longer in equilibrium. The correlation length at that time is the Kibble-Zurek length $l_{KZ}$. Consider a sweep that passes the critical point at $t = 0$. The idea of Kibble-Zurek scaling is that there is a scaling window $t, t' \in [-\tau_{KZ}, \tau_{KZ}]$ so that the nonequilibrium two-point function of an observable $\mathcal{O}$ satisfies

$$G_{\mathcal{O}}(t, t', k) = l_{KZ}^{\Delta_{\mathcal{O}}} g_{\mathcal{O}}\left(\frac{t + t'}{2\tau_{KZ}}; \frac{t - t'}{\tau_{KZ}}, k l_{KZ}\right), \quad (18)$$

where $g_{\mathcal{O}}$ is a universal function and $\Delta_{\mathcal{O}}$ is an anomalous dimension. In the following we will test Kibble-Zurek scaling by comparing equal time correlation functions computed for different quench rates.

We can define an instantaneous relaxation time $\tau(t)$ and correlation length $\xi(t)$. Near equilibrium dynamical scaling implies $\tau(t) \propto \xi(t)^z$. The Kibble-Zurek time can be obtained from the condition

$$\dot{\tau}(\tau_{KZ}) = 1, \quad (19)$$

which expresses the condition that the rate of change of the relaxation time is comparable to the relaxation time itself. In the following we will consider a specific protocol for changing the parameters of the model. The simplest possibility is to vary $m^2$ as a function of $t$. This is not the most general choice; in connection with simulating the dynamical evolution in the QCD phase diagram it is more appropriate to consider the evolution of both $m^2$ and $h$,

but the details of the trajectory depend on the precise embedding of the critical equation of state in QCD phase diagram [37].

Consider a power-law behavior for $m^2$ near the critical point, $\delta m^2 = \bar{m}^2 |\Gamma_Q \bar{t}|^{\tilde{a}}$. Here $\delta m^2 = m^2 - m_c^2$ and $\bar{t} = t - t_c$, where $t_c$ is the critical time, $m^2(t_c) = m_c^2$. We also defined the quench rate $\Gamma_Q$, the quench exponent $\tilde{a}$, and an amplitude $\bar{m}^2$. We then find

$$\begin{aligned}\dot{\tau}(t)|_{\bar{t}=\tau_{KZ}} &= \frac{d}{dt}\xi^z(t)\Big|_{\bar{t}=\tau_{KZ}} \\ &= \frac{d}{dt}(\delta m)^{-2z\nu}\Big|_{\bar{t}=\tau_{KZ}} \\ &= \frac{d}{dt}(\bar{m})^{-2z\nu}|\Gamma_Q \bar{t}|^{-z\nu\tilde{a}}\Big|_{\bar{t}=\tau_{KZ}} \\ &= (\bar{m}^{2/\tilde{a}}\Gamma_Q)^{-z\nu\tilde{a}}(\tau_{KZ})^{-(z\nu\tilde{a}+1)}, \end{aligned} \tag{20}$$

where $\nu \simeq 0.6299$ [34] is the correlation length exponent. This result determines the Kibble-Zurek time

$$\tau_{KZ} = (\bar{m}^{2/\tilde{a}}\Gamma_Q)^{-\frac{z\nu\tilde{a}}{z\nu\tilde{a}+1}}. \tag{21}$$

The corresponding Kibble-Zurek length is $l_{KZ} \propto \tau_{KZ}^{1/z}$. The simplest protocol for the evolution of $m^2$ is a linear sweep ($\tilde{a} = 1$) starting at $m^2(t=0) = m_0^2$. We use

$$m^2(t) = m_c^2 + (m_c^2 - m_0^2)\frac{t - t_c}{t_c} = m_c^2\left(1 + \frac{t - t_c}{\tau_Q}\right) \tag{22}$$

with $\tau_Q = \Gamma_Q^{-1} = t_c m_c^2/(m_c^2 - m_0^2)$. We initialize the system in the symmetric phase, $m_0^2 > m_c^2$. In practice we have used $m_0^2 = -2$ [recall that $m_c^2 = -2.28587(7)$]. The choice of $t_c$ then fixes the quench time $\tau_Q$. A scale for $\tau_Q$ is provided by the relaxation time $\tau_R$ of the slowest mode $k = 2\pi/L$ at criticality. The data in Fig. 2 correspond to a relaxation time $\tau_R \approx 2 \times 10^{-3} L^z$. In order to observe Kibble-Zurek dynamics we need to ensure that the slowest mode is equilibrated at the beginning of the sweep, but falls out of equilibrium as the critical point is approached. In the following we consider $\hat{\tau}_Q = (8, 4, 1, \frac{1}{4})$, where we have defined $\hat{\tau}_Q = \tau_Q/\tau_R$.

We observe that for a linear sweep the Kibble-Zurek time and length are given by

$$\tau_{KZ} \propto \tau_Q^{\frac{z\nu}{z\nu+1}} \simeq \tau_Q^{2/3} \propto t_c^{2/3}, \tag{23}$$

$$l_{KZ} \propto \tau_Q^{\frac{\nu}{z\nu+1}} \simeq \tau_Q^{1/6} \propto t_c^{1/6}. \tag{24}$$

In Fig. 6 we show the equal time correlation function of $\phi(t, \vec{x})$ as a function of the wave number $|\vec{k}|$ at a fixed instantaneous value of $m^2$ for different quench rates.

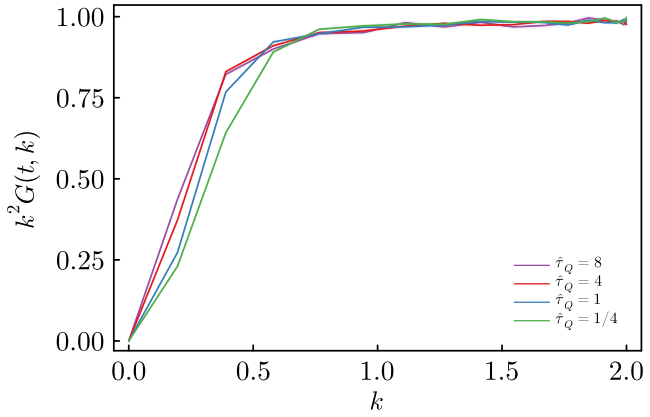


FIG. 6. Scaled equal time correlation functions $k^2 G(t_i; 0, k)$ obtained by sweeping the system from the high-temperature phase to an instantaneous value of $m^2(t_i) = -2.2145$ (slightly above the critical value $m_c^2 \simeq -2.2858$). We consider four different sweep times $\hat{\tau}_Q = (8, 4, 1, \frac{1}{4})$, where $\hat{\tau}_Q = \tau_Q/\tau_R$.

A simple model for the equal time two-point function in equilibrium is

$$G_{\rm eq}(0, k^2) = \frac{\chi_0(\xi/\xi_0)^{\gamma/\nu}}{1 + (k\xi)^{2-\eta}}, \tag{25}$$

where $\xi_0$ is the microscopic correlation length, $\chi_0$ the corresponding susceptibility, and $\gamma$ is the susceptibility exponent. The scaling relation $\gamma/\nu = 2 - \eta$ implies that the asymptotic form $G(0, k\xi \gg 1) \sim k^{-2+\eta}$ is independent of $\xi$. We note that $\eta \simeq 0.036$ is very small, and in practice we have normalized the correlation function to $G_0 \sim k^{-2}$ [38]. In a finite volume, the equal time correlation of model B is zero for $k = 0$. This is a consequence of charge conservation, and it is not seen in model A simulations.

Figure 6 shows the correlation functions at a fixed instantaneous value of $m^2 = -2.2145$. This value is close to (but slightly larger than) the critical value $m_c^2 \simeq -2.2858$. As explained above, we consider four different values of the quench time, $\hat{\tau}_Q = (8, 4, 1, \frac{1}{4})$. We observe that the correlation functions do indeed fall out of equilibrium, and that the effect is largest for the most rapid quench. In Fig. 7 we show that approximate Kibble-Zurek scaling holds; Data collapse is seen if $k$ is rescaled by $l_{KZ}$. Here we have treated the scaling exponent $p$ in the relation $l_{KZ} \propto \tau_Q^p$ as a free parameter. The best collapse for all $k l_{KZ}$ corresponds to $p \simeq 0.08$, compared to the prediction from Eq. (24), which gives $p \simeq 0.16$.

We note that Kibble-Zurek scaling is based on the fact that the correlation length is the only relevant length scale. On the lattice the microscopic length scale is given by the lattice spacing, and Kibble-Zurek scaling requires that $ka = 2\pi n(a/L) \ll 1$. In practice, this condition is only satisfied for the lowest modes on our lattice. Indeed, a $\chi^2$ fit to the exponent $p$, which emphasizes the regime of small $k$

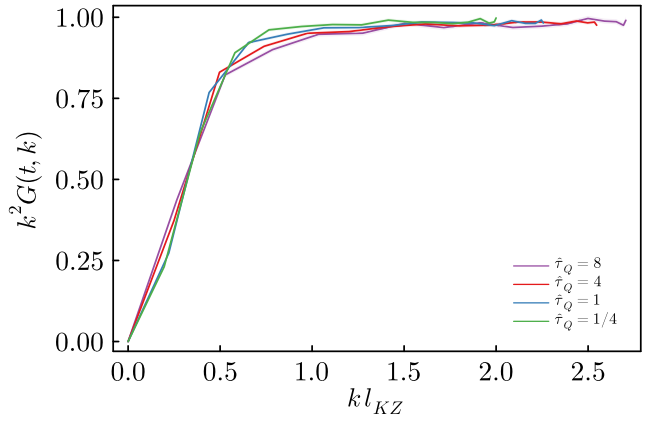


FIG. 7. Same as Fig. 6 as a function of the scaling variable $kl_{KZ}$ where $l_{KZ} \propto t_c^p$. In this figure we have used $p = 0.08$ to achieve the best data collapse for all values of $kl_{KZ}$. This value should be compared to the expectation in the scaling regime, $p = \frac{\nu}{z\nu+1} \simeq 0.16$.

where the statistical error is small, gives $p \simeq 0.16$. We conclude that a precise extraction of $p$ on a lattice with linear size $L = 32$ is difficult, and that a conservative estimate of $p$ is given by $p \simeq (0.08\text{–}0.16)$.

We have also studied the time evolution of the second moment of the order parameter in a finite volume during a sweep. This observable is related to the second cumulant that can be measured in relativistic heavy-ion collisions. We define

$$c_2(t,\tau_Q) = \left\langle \left( \frac{1}{V} \int_V d^3x \phi(x,t) \right)^2 \right\rangle_{\tau_Q}, \qquad (26)$$

where we take $V = (L^3)/2$ and we average over many sweeps with the same quench time $\tau_Q$. The result for different sweep rates is shown in Fig. 8. As expected, we observe that the slowest sweep rate leads to the largest

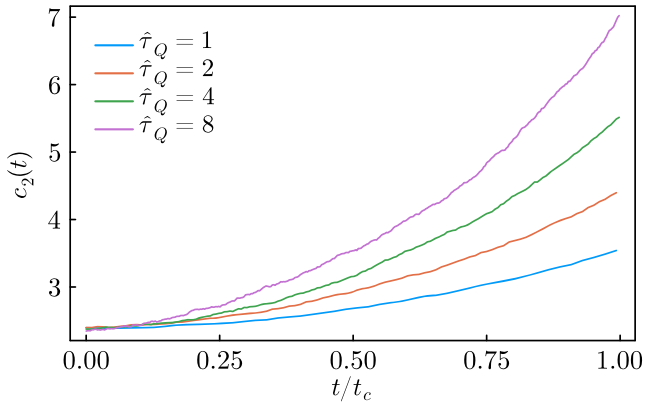


FIG. 8. Time evolution of the second moment $c_2(t,\tau_Q)$ of the order parameter integrated over a finite volume $V = (L^3)/2$. The different curves correspond to different sweep rates as indicated in the legend. The time is given in units of the critical time $t_c$ defined by $m^2(t_c) = m_c^2$.

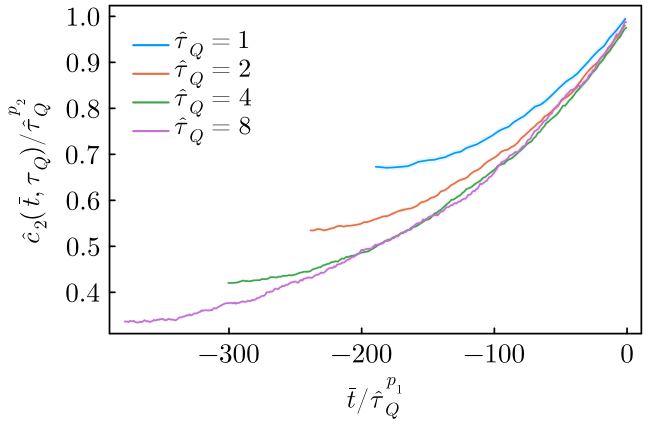


FIG. 9. This figure shows the rescaled second moment $\hat{c}_2(\bar{t},\tau_Q)/\hat{\tau}_Q^{p_2}$ as a function of $\bar{t}/\hat{\tau}_Q^{p_1}$. Here, we have defined $\hat{\tau}_Q = \tau_Q/\tau_R$ and the figure shows four different relaxation rates $\hat{\tau}_Q = 1$, 2, 4 and 8. In this figure we have used the mean-field critical exponents $p_1 = 2/3$ and $p_2 = 1/3$.

enhancement in $c_2(t,\tau_Q)$ near $t_c$. In order to check whether these results respect Kibble-Zurek scaling we first shift the time variable to $\bar{t} = t - t_c$. We also normalize $c_2(t,\tau_Q)$ to the value at $\bar{t} = 0$ and $\tau_Q = \tau_R$, and denote the normalized function $\hat{c}_2(\bar{t},\tau_Q)$.

We look for data collapse by plotting $\hat{c}_2(\bar{t},\tau_Q)/\hat{\tau}_Q^{p_2}$ against $\bar{t}/\hat{\tau}_Q^{p_1}$. The expectation from Kibble-Zurek scaling is $p_1 = \frac{z\nu}{z\nu+1}$ and $p_2 = \frac{2\nu}{z\nu+1}$. In Fig. 9 we show the evolution of the scaled moments for the mean field exponents $p_1 = 2/3$ and $p_2 = 1/3$. We observe approximate data collapse, but our data are not sufficiently accurate to distinguish between the mean field exponents and the prediction based on the full theory, $p_1 = 0.72$ and $p_2 = 0.36$.

## V. CONCLUSIONS AND OUTLOOK

We have performed numerical simulations of the diffusive dynamics of a conserved density (model B). The simulations are performed on a spatial lattice, and the time evolution is governed by a Metropolis algorithm. This algorithm is designed such that the first moment of the Metropolis step reproduces the diffusion equation, and the second moment matches the variance of the stochastic force. The Metropolis method also ensures that the equilibrium distribution is governed by the free energy functional even if the time step is not small.

The algorithm for the evolution of a conserved charge (model B) is based on updating fluxes and satisfies global charge conservation exactly. We have implemented this algorithm on a checkerboard which enables the update to be parallelized. The dynamical critical exponent in model B, $z \simeq 4$, is significantly larger than that on model A, $z \simeq 2$. This implies that it takes significantly longer to equilibrate or decorrelate model B configurations compared to

model A. Based on a finite size scaling analysis we were nevertheless able to obtain an accurate value of the dynamical exponent, $z = 3.972$, consistent with expectation $z = 4 - \eta$ from the dynamic renormalization group [5], combined with a determination of $\eta$ based on the conformal bootstrap [34].

In practical applications, for example when attempting to model the evolution of baryon number in relativistic heavy-ion collisions, we expect the system to fall out of equilibrium as the critical regime is approached. We have modeled this behavior by considering nonequilibrium sweeps of the mass parameter in the Ising free energy, starting from the high-temperature phase. We find evidence for approximate Kibble-Zurek scaling when we compare results for different sweep rates. This result both gives additional credence to our numerical methods, and it supports the use of Kibble-Zurek scale to estimate the maximum magnitude of critical fluctuations in far-from equilibrium systems.

There are several possible extensions and improvement of the work described here. One important goal is to couple stochastic diffusion to a fluid dynamic background that incorporates a realistic trajectory in the QCD phase diagram, and takes into account advection of the conserved density by the motion of the expanding fluid. A second objective is to include fluctuations in the fluid velocity. This corresponds to considering the dynamics of model H [5]. In this theory fluctuations of the order parameter couple to shear modes of the momentum density. Since the shear viscosity is only very weakly singular near the phase transition this coupling is expected to change the dynamical exponent to $z \simeq 3$, intermediate between the model A result $z \simeq 2$ and the model B exponent $z \simeq 4$.

## ACKNOWLEDGMENTS

We thank Katie Newhall and Derek Teaney for useful discussions. We acknowledge computing resources provided on Henry2, a high-performance computing cluster operated by North Carolina State University. This work is supported by the U.S. Department of Energy, Office of Science, Office of Nuclear Physics through the Contracts No. DE-FG02-03ER41260 (T. S.) and No. DE-SC0020081 (V. S.).

[1] M. A. Stephanov, K. Rajagopal, and E. V. Shuryak, Phys. Rev. Lett. **81**, 4816 (1998).
[2] A. Bzdak, S. Esumi, V. Koch, J. Liao, M. Stephanov, and N. Xu, Phys. Rep. **853**, 1 (2020).
[3] M. Bluhm *et al.*, Nucl. Phys. **A1003**, 122016 (2020).
[4] X. An *et al.*, Nucl. Phys. **A1017**, 122343 (2022).
[5] P. C. Hohenberg and B. I. Halperin, Rev. Mod. Phys. **49**, 435 (1977).
[6] D. Schweitzer, S. Schlichting, and L. von Smekal, Nucl. Phys. **B960**, 115165 (2020).
[7] T. Schäfer and V. Skokov, Phys. Rev. D **106**, 014006 (2022).
[8] B. Berdnikov and K. Rajagopal, Phys. Rev. D **61**, 105017 (2000).
[9] M. Nahrgang, M. Bluhm, T. Schäfer, and S. A. Bass, Phys. Rev. D **99**, 116015 (2019).
[10] D. Schweitzer, S. Schlichting, and L. von Smekal, Nucl. Phys. **B984**, 115944 (2022).
[11] D. T. Son and M. A. Stephanov, Phys. Rev. D **70**, 056001 (2004).
[12] K. Rajagopal and F. Wilczek, Nucl. Phys. **B399**, 395 (1993).
[13] E. Nakano, V. Skokov, and B. Friman, Phys. Rev. D **85**, 096007 (2012).
[14] A. Florio, E. Grossi, A. Soloviev, and D. Teaney, Phys. Rev. D **105**, 054512 (2022).
[15] S. Mukherjee, R. Venugopalan, and Y. Yin, Phys. Rev. C **92**, 034912 (2015).
[16] Y. Akamatsu, A. Mazeliauskas, and D. Teaney, Phys. Rev. C **95**, 014909 (2017).
[17] M. Stephanov and Y. Yin, Phys. Rev. D **98**, 036006 (2018).
[18] M. Martinez and T. Schäfer, Phys. Rev. C **99**, 054902 (2019).
[19] Y. Akamatsu, D. Teaney, F. Yan, and Y. Yin, Phys. Rev. C **100**, 044901 (2019).
[20] X. An, G. Başar, M. Stephanov, and H.-U. Yee, Phys. Rev. C **100**, 024910 (2019).
[21] X. An, G. Başar, M. Stephanov, and H.-U. Yee, Phys. Rev. C **102**, 034901 (2020).
[22] X. An, G. Başar, M. Stephanov, and H.-U. Yee, Phys. Rev. Lett. **127**, 072301 (2021).
[23] J. Berges, S. Schlichting, and D. Sexty, Nucl. Phys. **B832**, 228 (2010).
[24] G. Pihan, M. Bluhm, M. Kitazawa, T. Sami, and M. Nahrgang, Phys. Rev. C **107**, 014908 (2023).
[25] T. W. B. Kibble, Phys. Rep. **67**, 183 (1980).
[26] W. H. Zurek, Nature (London) **317**, 505 (1985).
[27] W. H. Zurek, Phys. Rep. **276**, 177 (1996).
[28] Y. Gao, K. Kirkpatrick, J. Marzuola, J. Mattingly, and K. A. Newhall, Commun. Math. Sci. **19**, 453 (2021).
[29] P. J. Rossky, J. D. Doll, and H. L. Friedman, J. Chem. Phys. **69**, 4628 (1978).
[30] G. O. Roberts and J. S. Rosenthal, J. R. Stat. Soc. Ser. B **60**, 255 (1998).
[31] G. D. Moore, Nucl. Phys. **B568**, 367 (2000).
[32] M. Hasenbusch, Phys. Rev. E **101**, 022126 (2020).
[33] J. Zinn-Justin, *Quantum Field Theory and Critical Phenomena*, International Series of Monographs on Physics Vol. 113 (Oxford Science Publications, Oxford, England, 2002).

[34] S. El-Showk, M. F. Paulos, D. Poland, S. Rychkov, D. Simmons-Duffin, and A. Vichi, J. Stat. Phys. **157**, 869 (2014).
[35] L. F. Alday and A. Zhiboedov, J. High Energy Phys. 06 (2016) 091.
[36] A. Chandran, A. Erez, S. S. Gubser, and S. L. Sondhi, Phys. Rev. B **86**, 064304 (2012).
[37] P. Parotto, M. Bluhm, D. Mroczek, M. Nahrgang, J. Noronha-Hostler, K. Rajagopal, C. Ratti, T. Schäfer, and M. Stephanov, Phys. Rev. C **101**, 034901 (2020).
[38] Note that the value of $\eta$ is the same in model A and B, but the large value of $z$ in model B implies that a numerical calculation of $\eta$ requires fewer resources in model A than it does in model B.